A simple approach to synthesize g-C_3N_4 with high visible light photoactivity for hydrogen production

P. Martín-Ramos[a], J. Martín-Gil*[a], R. C. Dante[a], F. Vaquero[b], R.M. Navarro[b], J.L.G. Fierro[b]

[a] Advanced Materials Laboratory, ETSIIAA, University of Valladolid, Avenida de Madrid 44, 34004 Palencia, Spain. Tel: +34 (979) 108347; e-mail: jesusmartingil@gmail.com.

[b] Institute of Catalysis and Petrochemistry, CSIC, Cantoblanco, 28049 Madrid, Spain. Fax: +34 91 585 477; e-mail: r.navarro@icp.csic.es.

Abstract. Se-modified g-C_3N_4 was synthesized from sonicated aqueous suspensions of melamine cyanurate and SeO_2. The different thermal condensation temperatures in the 500-650 ºC range were found to influence the photophysical properties and hydrogen evolution rates. H_2 evolution increased dramatically by two orders of magnitude when Pt co-catalyst (1 wt.%) was incorporated, reaching an HER of 75 μmol H_2/h.

Keywords: carbon nitride; hydrogen generation; selenium; water-splitting.

1. INTRODUCTION

To make a true contribution to the energy supply, the diluted solar energy must be captured, converted and stored as highly structured electronic energy in chemical bonds. As this is done in nature by photosynthesis, an approach for mimicking photosynthesis is the generation of O_2 and H_2 via water splitting. However, as direct water splitting cannot be achieved by sunlight because water molecules are not electronically excited by sunlight photons, appropriate systems have been developed to absorb efficiently the solar energy to produce the water splitting reaction in an indirect way [1-6]. In this concept, sunlight is absorbed by light harvesting semiconductors producing spatially separated electron-hole pairs that, if not recombined, can reduce and oxidize water molecules.

The search for efficient photocatalysts under visible light has grown exponentially along the last few years. Suitable photocatalysts to split water into H_2 and O_2 at reasonable efficiency have relied on the use of prohibitively expensive light-absorbing semiconductors [7], e.g., GaInP and (Al)GaAs, and/or co-catalysts (Pt, Rh, IrO_2) and strong acidic or basic reaction media, which are difficult to manage over the large areas needed for light harvesting. Thus, great effort has been made recently with the aim of developing photocatalysts including in their composition earth-abundant elements, able to operate closely to neutral pH values. Achievements have included not only the discovery of new active photocatalysts but also the development of innovative strategies to enhance the reactivity of known photocatalysts. Among the later approaches, doping, mainly anionic [8-10], was widely investigated along the last few years because of its effectiveness in bandgap engineering, and therefore in broadening the light responsive range of wide-bandgap semiconductors [11-14].

Before 2009, all visible-light photocatalysts active in water reduction and oxidation reactions were metal-based inorganic solids, such as metal oxides, metal-(oxy)nitrides, and metal-oxysulfides [11-16], primarily due to the lack of a material with appropriate band-edge positions and adequate stability during photocatalysis. Since that, Wang *et al.* [17] reported that graphitic carbon nitride (g-C_3N_4) with a band gap of 2.7 eV was a good photocatalyst for water-splitting applications. This semiconductor can be synthesized by thermal polycondensation of common organic monomers (e.g., cyanamide). Its graphitic planes are constructed from tri-s-triazine units connected by planar amino groups. The in-plane organization of tri-s-triazine units enables the generation of carbon nitride polymers with adjustable electronic properties. The as-prepared g-C_3N_4 powder achieved functionality as a stable photocatalyst for H_2 evolution from water

containing an appropriate electron donor under visible-light irradiation (>420 nm), even without using a co-catalyst [18-20]. However, the lack of absorption above 460 nm of g-C_3N_4 requires additional techniques to utilize the visible region more effectively. Therefore, expanding light absorption of g-C_3N_4 up to a large portion of the solar spectrum becomes imperative. Among the methods proposed to solve this limitation of g-C_3N_4, its doping with non-metallic elements such as P [21], S [22], F [23], and B [24] has been proposed.

Herein, we report our successful attempt to introduce selenium atoms into g-C_3N_4 by a simple procedure that consists in sonication of aqueous suspensions of the precursors (melamine cyanurate and SeO_2) and a subsequent thermal treatment at temperatures between 500 and 650 °C. This approach provides an easy way to modulate the bandgap structure and shows an extremely high H_2 production rate under visible light irradiation when 1.0 wt.% Pt is added as co-catalyst.

2. EXPERIMENTAL

2.1. *Materials and synthesis procedure*

The reagent, melamine cyanurate (MCA), was supplied by Nachmann S.r.l. (Milan, Italy) with purity higher than 99%. This precursor (MCA) was mixed with SeO_2 (CAS No. 7446-08-4, Sigma Aldrich, >99.9%) in molar ratio 3:1 (69 g of sample were mixed with 10 g of SeO_2 in 0.8 L of water) in a beaker and sonicated for 50 min at room temperature, leading to a suspension with pH 1.5. This suspension was allowed to stand for 12 h, and then was dried in a vacuum oven at 200 ºC for 6 h (the precursor is deliquescent and hygroscopic). Samples of the dry solid (slightly reddish) were ground in an agate mortar, were placed in a sealed Vycor® glass vial with a valve and were thermally treated at different temperatures for 50 min in a convective tubular oven GVA 12/900, power: 5.460 kW, heating length: 900 mm, T_{max}: 1200 ºC (Carbolite, UK) under nitrogen flow. The heating and cooling rates were 10 ºC/min. The polymerization-condensation reaction for the Se-free g-C_3N_4 sample, prepared directly from bare MCA, was conducted following the same thermal treatment program.

The reaction yields were: 21.15% at 500 ºC, 18.70% at 550 ºC, 16.93% at 600 ºC and 13.22% at 650 ºC (and then dramatically dropped to ca. 1% at 700 ºC). For comparison purposes, the reaction yield for the g-C_3N_4 sample obtained from bare MCA was 17.35 %.

The colour of the samples evolved from orange red (500 ºC) to yellow orange (550 ºC), to pale yellow (600-650 ºC) and finally to brown (700 ºC).

With regard to the role of selenium, it would act as a catalyst for the polycondensation reaction: SeO_2 is a strong oxidant and, since it is an acidic oxide, it reacts with water to yield H_2SeO_3. Selenous acid plays a similar role to that of H_2SO_4 when it interacts with melamine cianurate, that is, a dehydration reaction takes place and the following reaction is promoted [25]:

$$C_3N_3(NH_2)_3 \cdot C_3N_3(OH)_3 \rightarrow C_6N_7(NH)(NH_2) + 3H_2O$$

It should be noted that SeO_2 is highly toxic and that all the synthetic procedures should be conducted in a fume hood.

2.2. *Characterization*

The content of carbon, nitrogen and hydrogen was determined by means of a Carlo Erba analyser CHNS-O EA 1108. This analysis method is based on the complete and instantaneous oxidation of the sample by “flash combustion”.

The specific surface areas of the catalysts were calculated by applying the BET method to the N_2 adsorption/desorption isotherms measured at liquid nitrogen temperature (-196 ºC) on a Micromeritics TRISTAR 3000 instrument, using samples previously degassed under vacuum (ca. 10^{-4} mbar) at 120 ºC for 2 h to remove all moisture and gases adsorbed on the surface of the

samples. The specific surface area values of the samples were calculated by applying the BET equation to the nitrogen adsorption isotherm within the relative pressures $0.05 < P/P_0 < 0.30$.

X-ray diffraction patterns were obtained using an ENRAF-NONIUS FR590 powder diffractometer equipped with an INEL CPS 120 detector (Debey-Scherrer geometry), using Cu Kα radiation and glass capillaries for sample mounting.

Infrared spectra were recorded by means of a Thermo Nicolet 380 Fourier transform-infrared (FT-IR) spectrophotometer using KBr pellet method, in order to identify the chemical functional groups.

Scanning electron microscopy (SEM) images were collected with a FEI - Quanta 200FEG equipped with a Genesis energy-dispersive X-ray (EDS) spectrometer system. Transmission electron microscope (TEM) micrographs were collected with a JEOL JEM-FS2200 HRP equipped with an Oxford instruments INCA Energy TEM 250 EDS probe.

X-ray photoelectron spectra were acquired with a VG-Escalab 200R spectrometer, equipped with a hemispheric electron analyser (constant pass energy of 50 eV) and a Mg Kα (1253.6 eV) X-ray source powered at 100 watts. High resolution C1s, N1s, Se3d and Pt4f core-level spectra were recorded in increments of 0.07 eV with dwell times of 40 ms. Charge effects were corrected with respect to the C1s peak of adventitious carbon at 284.8 eV. High-resolution spectra envelopes were obtained by curve fitting synthetic peak components using the "XPS peak" software and using symmetric Gaussian-Lorentzian lines to approximate the line shapes of the fitting components. An "S" shaped background was considered in the fitting of spectra.

The diffuse reflectance spectra of the samples were obtained by means of a UV-vis Jasco V-670 equipped with an integrating sphere. An analysis of the reflectance spectra was carried out to obtain the bandgap following the method of the Kubelka-Munk function F(R). The bandgap values were calculated by the Tauc plot method [26,27].

2.3. *Photocatalytic Activity Measurements*

Photocatalytic activity was determined in a closed Pyrex glass reactor (200 mL) working at room temperature under Ar at atmospheric pressure. The photocatalyst powder (0.050 g) was dispersed by ultrasonic sonication for 30 min in an aqueous solution (150 mL) containing triethanolamine as a sacrificial reagent (TEA 10% vol). Before measurement, the solution was purged several times with Ar to ensure complete air removal. The modification of the g-C_3N_4 photocatalysts with Pt co-catalyst (1 wt.%) was done by *in-situ* photoreduction using a Xe arc lamp (150 W) and hydrochloric platinum acid (H_2PtCl_6) mixed with the photocatalyst in the reaction solution before adding the sacrificial reagent. The *in-situ* photoreduction process with irradiation takes about 3 h. The photocatalysts were irradiated for 5 h with an ozone-free 150 W Xe arc lamp (LOT Oriel GmbH& CO KG) equipped with a cut-off filter for visible only radiation (Schott GG455, λ>455 nm). Samples of the evolved gases were extracted periodically and analysed by GC with TCD (Varian chromatograph Model Star 3400 CX) equipped with a 5A molecular sieve using Ar as carrier gas. Photoactivity results are presented in terms of rate of hydrogen production (μmol/h) during irradiation time (5 h).

3. RESULTS AND DISCUSSION

3.1. *Elementary analysis and textural data*

From Table 1 it can be confirmed that the C/N ratio approached its ideal value (0.75) as the temperature was increased, in good agreement with the values obtained from XPS data (0.72) and EXD data (0.71) reported below. It is also worth noting that the C/N ratios for all samples were similar to those previously reported for their analogous bare MCA samples [25] and that the Se content (obtained from EDS analysis) was drastically reduced as the treatment temperature was increased.

Table 1. Summary of CHN elementary analysis results for the Se-modified samples treated at different temperatures. The Se content has been obtained from EDS data.

Samples	N (wt%)	C (wt%)	H (wt%)	Se (wt%)	N (mol)	C (mol)	C/N ratio	N/C ratio
g-C_3N_4 @ 500ºC	51.62	29.02	1.99	9.84	3.6856	2.4161	0.656	1.525
g-C_3N_4 @ 550ºC	59.60	33.94	1.93	3.24	4.2551	2.8260	0.664	1.506
g-C_3N_4 @ 600ºC	61.41	35.57	1.52	1.07	4.3846	2.9615	0.675	1.481
g-C_3N_4 @ 650ºC	61.33	35.89	1.48	0.45	4.3786	2.9885	0.683	1.465

Textural data of g-C_3N_4 samples showed that the specific surface area developed by the photocatalysts varied with the condensation temperature used in the synthesis (2). An increase was observed in the specific surface area of the Se-modified g-C_3N_4 samples as the temperature of condensation was increased. This increase can be assigned to development of the mesoporous structure of the samples associated to changes in the size and morphology of the g-C_3N_4 samples induced by the increase of condensation temperature.

Table 2. Specific surface area developed by Se-modified g-C_3N_4 samples treated at different temperatures. The BET for g-C_3N_4 prepared from bare melamine cyanurate (MCA) is also included for comparison purposes

Reactant	Samples	BET (m^2/g)
MCA + H_2SeO_3	g-C_3N_4 @ 500ºC	31.9
	g-C_3N_4 @ 550ºC	51.7
	g-C_3N_4 @ 600ºC	70.2
	g-C_3N_4 @ 650ºC	68.7
MCA	g-C_3N_4 @ 650ºC	83.3

3.2. *X-ray powder diffraction*

Direct evidence of the structure of the g-C_3N_4 photocatalyst was revealed by XRD. The XRD patterns of the samples condensed at 500, 550, 600 and 650 ºC show two distinct diffraction peaks around 27.4º (intense) and 13.0º (weak) (Figure 1, *left*). The sample pretreated at 500 ºC displays a broad peak around 27.4°, corresponding to the 002 reflection with interplanar distance of 3.25 Å. Above 550 °C this peak is shifted towards 27.9°, which corresponds to the 002 reflection with an interplanar distance *c*/2 of 3.21 Å, a typical value of polymeric C_3N_4. The tightening of the interplanar distance from 3.25 Å to 3.21 Å (3.19 Å at 650 °C) is probably due to a much stronger interplanar interaction, such as a contribution of a π-interplanar bond [28,29].

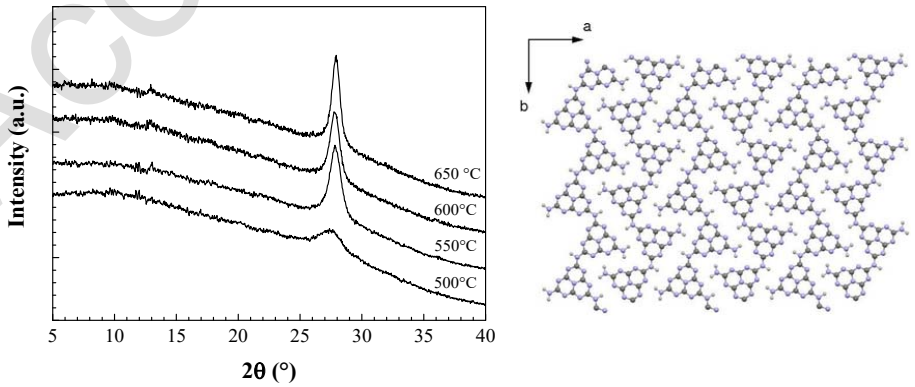

Figure 1. Powder X-ray diffraction patterns of Se-modified g-C_3N_4 samples treated at different temperature (*left*); In-plane view of a sheet of polymeric carbon nitride (*right*).

The other characteristic peak, located at ca. 13º (interplanar distance of 6.9 Å), is generally weak and originates from the in-plane reflections [30,31].

3.3. *Infrared spectroscopy*

Some other structural features are provided by FTIR spectroscopy. The FT-IR spectra of the g-C_3N_4 samples condensed at temperatures within the 500-650 ºC are displayed in Figure 2. These spectra correspond to the so-called *melon*, i.e. polymeric carbon nitride (see Figure 1, *right*), which is known to consist of heptazine units. They show bands in the 3500-3000 cm^{-1} region associated to NH stretching vibration modes and a few bands in the 1640-800 cm^{-1} region. These later bands are assigned to conjugated CN stretching (1637 cm^{-1}), stretching of the tri-s-triazine ring (from 1574 to 1459 cm^{-1}), secondary bridging N (all associated with the four NH stretching bands) and primary amines (from 1400 cm^{-1} to 1204 cm^{-1}). The small but sharp peak at 892 cm^{-1}, that grows from 500 ºC to 650 ºC, is associated to a deformation mode of cross-linked heptazine deformation, whereas that at 813 cm^{-1} is characteristic of a tri-s-triazine ring mode of bending [30,31]. Peak sharpening and definition with increasing temperature is likely due to the stacking arrangement, as it can be inferred from XRD measurements.

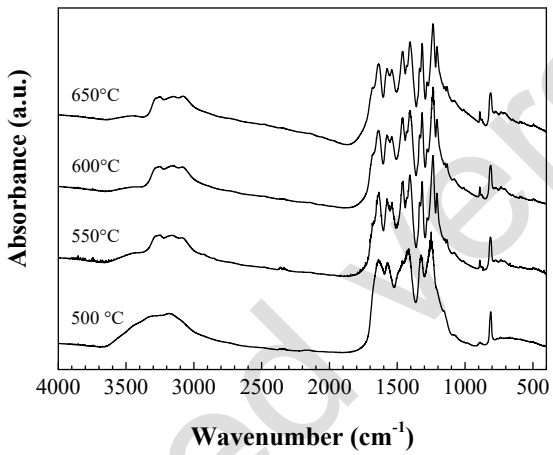

Figure 2. FT-IR spectra of Se-modified g-C_3N_4 samples treated at different temperatures.

3.4. *Textural properties and EDS analysis*

The texture of the Se-modified g-C_3N_4 samples was studied by SEM and TEM. Figure 3 shows SEM micrographs of a representative Se-modified g-C_3N_4 sample treated at 650 ºC, bare (Figure 3, *left*) and after Pt co-doping (Figure 3, *right*). Samples treated at 550 and 600 ºC showed similar textural properties. It can be observed that the nanosheets of polymeric carbon nitride tend to form crumpled surfaces. These conformations seem to originate from the curled surfaces, which tend to enrol and then shrink. Conversely, the sample treated at 500 ºC (not shown) exhibits slightly more interconnected flakes, in close agreement with the morphological features previously reported for sulphuric acid treated g-C_3N_4 samples [25].

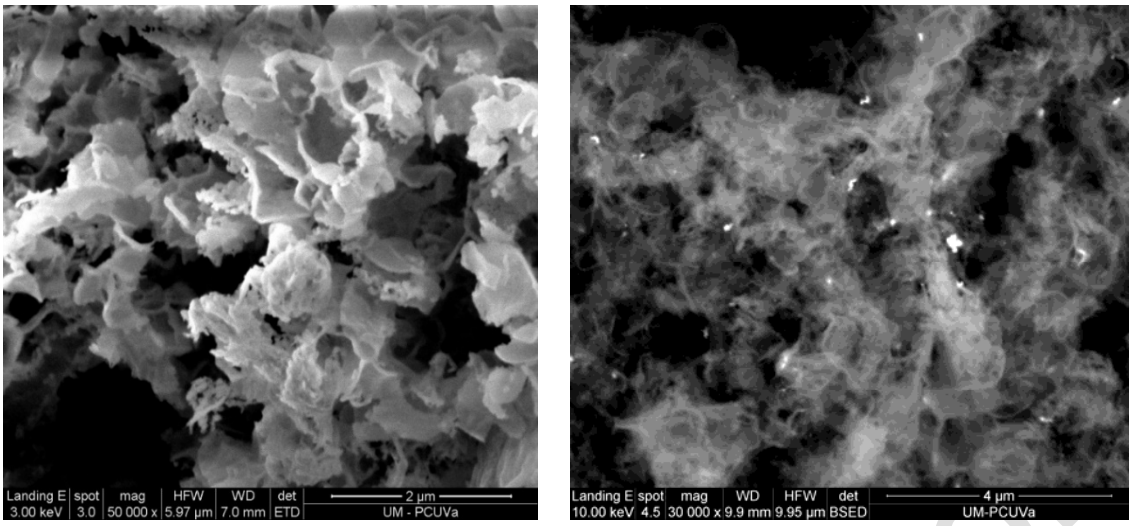

Figure 3. SEM images of a Se-modified g-C_3N_4 sample treated at 650 °C: (*left*) bare sample; (*right*) sample co-doped with 1 wt.% Pt co-catalysts.

The improvement of the activity associated to the presence of Pt co-catalyst depends on the interface/junctions between the light harvesting semiconductor and the co-catalyst (see Section 3.7). Therefore a high dispersion of Pt co-catalyst on g-C_3N_4 is essential so as to attain efficient collection of photoinduced charges because the formation of atomically well-defined junctions between Pt and g-C_3N_4 might facilitate charge transfer between g-C_3N_4 and Pt. TEM micrographs (Figure 4) show good dispersion of Pt nanocrystals in the g-C_3N_4 flakes.

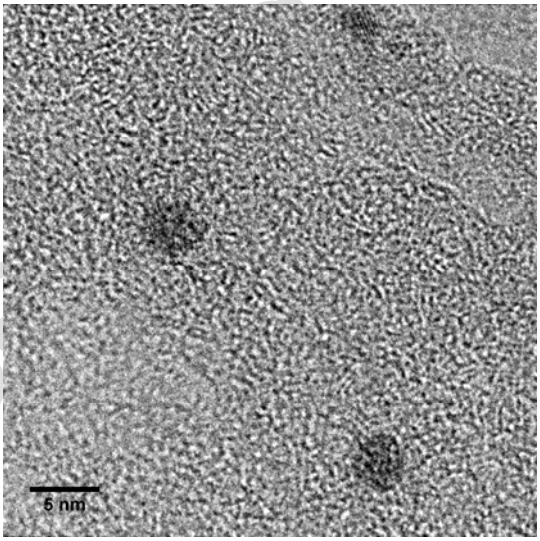

Figure 4. TEM micrographs of the Se-modified g-C_3N_4 sample treated at 650 ºC co-doped with 1 wt.% Pt

The EDS analysis was conducted both on top of a regular carbon conductive tab and using an aluminium sample holder, so as to avoid inaccuracies in the C percentage estimation (see Figure S1[†]). The analysis data is summarized in Table 3. The C/N ratio is 0.708, in good agreement with the elementary analysis and XPS data. The selenium doping is 0.45 wt. %. The Pt co-doping (0.98 wt. %) is very close to the desired value (1 wt. %).

Table 3. EDS analysis results for Se-modified g-C_3N_4 treated at 650 ºC, with Pt co-doping

Element	Wt %	At %
C K	36.89	41.21

N K	60.73	58.18
Se L	00.45	00.08
Al K (*)	00.94	00.47
Pt M	00.98	00.07

(*) Contribution from the sample holder.

3.5. *X-ray photoelectron spectroscopy analysis*

Photoelectron spectroscopy (XPS) was undertaken with the aim of accurately determining the chemical bonding, surface structure and relative abundance of the elements in the surface region (thickness 2-3 nm) of the samples. All samples displayed strong C1s and N1s emissions, in agreement with previous studies [32,33], and a very weak Se3d line together with residual O 1s peak. Table 4 reports the different binding energies detected in C1s, N1s and Se3d core-levels and the assignment of the chemical species originating them.

Table 4. Peak assignment of core-levels of Se-modified g-C_3N_4 samples

Core-level	Binding energy (eV)	Assignment	Reference
C1s	284.8 287.8 289.4 293.5	sp^2 C-C C-$(N)_3$ C(O_2) $\pi \rightarrow \pi^*$	[34,35] this work
N1s	398.6 399.8 401.5	sp^2 (C=N-C) N-$(C)_3$ C-N-H	[35-38] this work
Se3d	55.4	Se-C	[39]

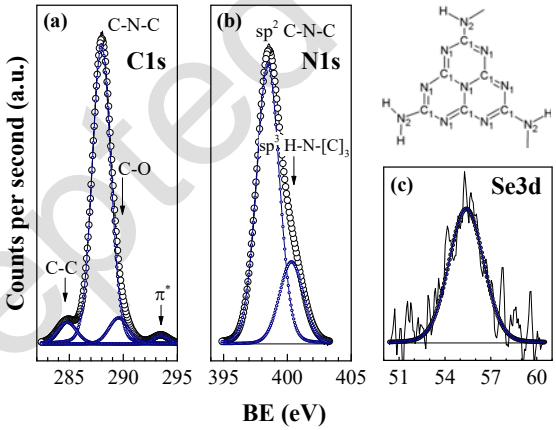

Figure 5. (*a*) C1s, (*b*) N1s and (*c*) Se3d core-level spectra of the Se-modified g-C_3N_4 sample condensed at 650 °C with associated deconvolution components. The scheme of the equivalent atoms in the polymer repeating-unit as determined by XPS spectra is shown in the upper right corner. Larger open circles correspond to experimental data; smaller solid circles belong to theoretical fittings; the noisy line in (*c*) is the experimental spectrum.

The C1s core-level spectra displayed in Figure 5a show an intense component at 287.8 eV, a shoulder around 289.4 eV and a very weak feature at ca. 293.5 eV. The former component is attributed to the C-atoms belonging to the heptazine ring while the shoulder is likely originated from an electron-rich C-O environment, such as in COO species, and that at 293.5 eV is due to excited electrons of the π* orbital of the heptazine units (Table 4). Samples also exhibited a small component at 284.8 eV, which is typical of C-C bonding of contamination. The XPS data gave an evidence for the existence of graphite-like sp^2-bonded structure in graphitic carbon nitride. Similarly, the N1s peak was deconvoluted and two clear components at 398.5 and 400.3 eV were found. They correspond to sp^2 C-N-C and sp^3 H-N-$[C]_3$ groups, respectively (Table 4).

Some of the samples also displayed a very weak feature somewhere around 404.1 eV, usually assigned to terminal nitrates and/or excited π* orbital as for carbon. Atomic C/N percentages derived from XPS measurements resulted 0.72, which is close to the nominal composition of g-C_3N_4 (C/N=0.75) and to the values obtained from elementary analysis (Table 1) and EDS analysis (Table 3), and remained virtually unchanged within the temperature range 500-650 ºC.

The equivalent atoms of the repeating polymer unit are presented in Figure 5b, as determined by XPS results. N1, N2 and C1 correspond to the deconvolution curves with peaks at 398.5, 400.3, and 287.8 eV, respectively. It is worth mentioning that the existence of selenium within the framework of g-C_3N_4 is clearly evidenced by measuring the Se3d core-level spectra (Figure 5a). A weak signal at 55.4 eV was recorded for the 600 and 650 ºC treated samples. This signal is noisy because the Se loading is 1.07 and 0.45 wt.%, respectively (Table 3). The binding energy of $Se3d_{5/2}$ emission in organic compounds containing C-Se bonds was recognized as 55.6 eV [39]. Thus, the peak at 55.4 eV is reasonably considered to be originated from C-Se bonds formed in g-C_3N_4 samples by substituting lattice nitrogen for Se atoms. The Se/C atomic ratios for the samples pretreated at 500 ºC and 550 ºC are 0.002 and 0.001, respectively, and decrease to the level of traces in the samples pretreated at the highest temperatures.

3.6. *Electronic and optical gap characteristics from UV-Vis spectra*

Condensation temperature remarkably changed the optical properties of the Se-modified g-C_3N_4: the UV-Vis spectra of Se-modified g-C_3N_4 samples treated at temperatures in the 500 to 650 °C range are depicted in Figure 6. It is worth pointing out that, apart from the large band with a maximum around 390 nm, a considerable and well-defined shoulder appears above 400 nm. This is due to electrons whose energy is located between the valence and conduction band [40]. The found bandgaps E_g (calculated by Tauc plot method with exponent r =1/2) [26,27] are 2.85 eV for the samples treated at 500 and 550°C, 2.75 eV for the sample treated at 600°C and 2.9 eV for that treated at 650°C, which are typical values of a wide-band gap semiconductor [29]. However, another transition was found between 2 and 2.25 eV, related to a marked shoulder at 480 nm. These electrons are much closer to the conduction band, in accordance to the fact that the material is an *n*-type semiconductor, as determined by other means by Zhang *et al*. [22]. It is also noteworthy that the sample treated at 500 °C exhibited a broad band centred around 550 nm, which could tentatively be connected to the interaction with Se (still present in a larger amount, 9.84 wt.%, at that treatment temperature). As the treatment temperature was increased, the broad band was shifted to lower wavelength values and seems to be more connected to the polymerization process rather than directly to Se, since the spectra are similar to those observed for bare MCA samples, as described in a previous paper by Dante *et al*. [25]. The lowest transition (2-2.25 eV) has been interpreted by Jorge *et al*. as a π→π* transition involving N lone pairs [40], allowed as increased condensation causes distortion of the polymeric units.

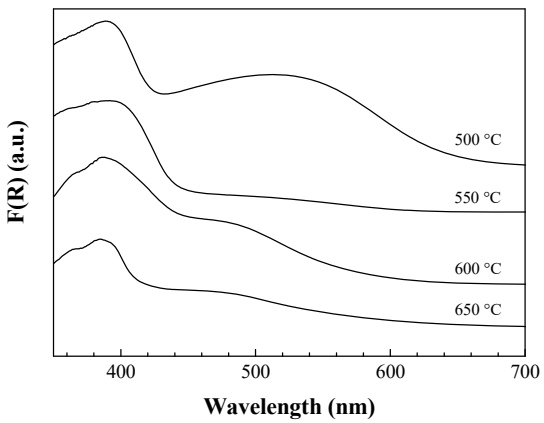

Figure 6. UV-vis spectra of Se-modified g-C_3N_4 samples treated at different temperatures.

3.7. *Photocatalytic activity measurements*

Photocatalytic hydrogen evolution over different g-C_3N_4 samples -either alone or loaded with 1.0 wt.% of Pt- was evaluated under visible light irradiation (>465 nm) using triethanolamine (TEA) as a scavenger, at room temperature and atmospheric pressure following a procedure similar to a previously reported method [13]. Prior to catalyst testing, blank experiments showed that no reaction occurs when the system was illuminated in the absence of catalyst or in the presence of catalyst without illumination. Table 5 summarizes the hydrogen production rate obtained over Se-modified g-C_3N_4 samples synthesized at different temperatures and over bare (Se-free) MCA treated at 650 ºC for comparison purposes.

Table 5. Rates of hydrogen production under visible-light irradiation over g-C_3N_4 photocatalysts condensed at different temperatures (without and with 1wt% Pt).

Reactant	Samples	Without Pt co-catalyst		With Pt co-catalyst	
		HER (μmol H_2/h)	Surface normalized HER (μmol H_2/m^2 h)	HER (μmol H_2/h)	Surface normalized HER (μmol H_2/m^2 h)
MCA + H_2SeO_3	g-C_3N_4 @ 500ºC	0.066	0.041	3.34	2.09
	g-C_3N_4 @ 550ºC	0.033	0.013	55.70	21.54
	g-C_3N_4 @ 600ºC	0.018	0.0045	57.75	17.08
	g-C_3N_4 @ 650ºC	0.1025	0.030	75.03	21.85
MCA	g-C_3N_4 @ 650ºC	0.735	0.176	46.60	11.18

The as-prepared Se-modified g-C_3N_4 samples showed low H_2 production rates (Table 5). A decrease in the hydrogen production rate was observed with the increase in the temperature of condensation up to 600 ºC. For the sample condensed at 650ºC, a sharp increase in photoactivity was observed. This indicates that changes in the structure and surface characteristics of g-C_3N_4 play a determinant role in its photocatalytic activity towards H_2. The surface area of g-C_3N_4 samples is a parameter to be taken into account when analyzing their photoactivity behavior because higher specific surface areas imply higher light absorption capacity and higher number of surface centers for reaction. Figure 7a represents the rate of hydrogen production normalized per surface area of g-C_3N_4. From this figure it can be observed that g-C_3N_4 samples presented differences in the surface-normalized production rates, which implies that there are characteristics beyond the surface of photocatalysts that affect their photoactivity. According to previously discussed physicochemical characterization of g-C_3N_4 samples, the condensation temperature also remarkably changed the optical properties of the g-C_3N_4 samples. However, no direct correlation was found between the photo-optical properties of the g-C_3N_4 samples and their surface-normalized production rates. From these observations, it appears that photoactivity values of bare g-C_3N_4 samples are sensitive to surface features (surface composition and/or possible preferential exposure of specific surface facets possessing unique photoactivity).

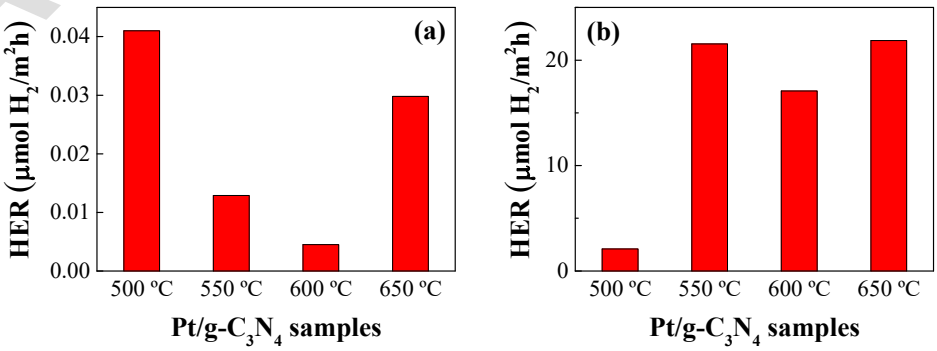

Figure 7. Rates of hydrogen production under visible-light irradiation (normalized per surface area) over Se-modified g-C_3N_4 photocatalysts condensed at different temperatures, without Pt (*a*) and with 1 wt.% Pt (*b*).

The modification of the samples with Pt provoked a dramatic enhancement of their photocatalytic activity (Table 5, Figure 7b). In particular, the incorporation of Pt to the Se-modified g-C_3N_4 samples treated at 550, 600 and 650 ºC enhanced their rates of hydrogen production by two orders of magnitude respect to the bare g-C_3N_4 counterparts. The stability of the Pt/g-C_3N_4-650 sample was studied by analyzing its photocatalytic behavior in light on/light off cycles. No signs of deactivation were observed after 5 cycles. As discussed above, in the absence of Pt nanoparticles, the H_2 evolution rates on bare g-C_3N_4 samples are low, which indicates that the Schottky effect plays an important role in capturing excited electrons generated on the photocatalyst [41]. An enhancement of hydrogen production activity (by a factor of ~750) by the presence of a small amount of metallic Pt had already been reported by Shi *et al*. [42]. The enhancement in photoacitivy can be explained in terms of charge transfer promotion and creation of hydrogen desorption sites [42]. Concerning the role of Pt co-catalyst facilitating the electron transfer, it is necessary to achieve a good contact degree between the surface of the noble metal entities and the g-C_3N_4 particles. Taking into account that platinization effect on g-C_3N_4 samples greatly boosted hydrogen production on the samples annealed at temperatures higher than 500 ºC, this indicates that the formation of g-C_3N_4 plays a determinant role for the enhancement of its photocatalytic activity when Pt is present on their surfaces. Formation of well-defined junctions between g-C_3N_4 surface and Pt particles could enhance the electronic transfer between both phases. This increases the efficiency of water splitting by decreasing the probability of electron-hole recombination.

The presence of selenium would also play a role in the photocatalytic performance because the comparison of the photoactivities of the Se-modified/Se-free samples treated at 650ºC (75.03 *vs*. 46.60 μmol H_2/h, respectively, see Table 5) evidenced an improved activity of the platinized samples when selenium was present on the g-C_3N_4 sample. This would be in agreement with the experimental results [43-45] and *ab-initio* calculations [46,47] for analogous sulphur-doped samples, so a similar enhancement mechanism can be tentatively suggested. Apart from the changes in the bulk lattice of g-C_3N_4 observed on Se-modified samples, the possible role of selenium species on the surface, altering the surface platinum dispersion or modifying the surface adsorption of H_2O and TEA, could be discarded because the XPS surface analysis of g-C_3N_4 samples (Table 4) showed a decrease in the surface concentration of Se with the increase in the condensation temperature, that is contrary to the increase in the rate of hydrogen production observed in Figure 7b.

4. Conclusions

Se-modified g-C_3N_4 photocatalysts loaded with 1 wt.% Pt co-catalyst have been synthesized and their photocatalitic activity was tested in the H_2 evolution from water under visible light irradiation. These photocatalysts exhibited very stable and drastically enhanced photocatalytic hydrogen production, and their excellent performance suggests that the formation of well-defined junctions between Se-doped g-C_3N_4 surface and Pt particles enhance the rate of electron transfer between both phases. The results acquired may shed light on general doping strategies for designing potentially efficient photocatalysts.

5. Acknowledgments

The authors gratefully acknowledge the support of Dr. Manuel Avella (Microscopy Unit, Parque Científico, Universidad de Valladolid) and Dr. Francisco M. Sánchez-Arévalo (IIM-UNAM) with the SEM and TEM analysis and the DR spectra measurements, respectively. P. Martín-Ramos would like to thank Iberdrola Foundation for its financial support. UVa group acknowledges financial support of Junta de Castilla y León through project VA036A12-2. ICP-CSIC group acknowledges the research program supported by the Secretaría de Estado de Investigación, Desarrollo e Innovación (MINECO, Spain) under the project CTQ2013-48669-P.

6. Appendix A

† Electronic Supplementary Information (ESI) available: EDS analysis for Se-modified g-C_3N_4 treated at 650 ºC. See DOI: XXXXXXXXXX

7. References

[1] Yi Z, Ye J, Kikugawa N, Kako T, Ouyang S, Stuart-Williams H, et al. An orthophosphate semiconductor with photooxidation properties under visible-light irradiation. Nature Mater. 2010;9:559-64.

[2] Maeda K, Higashi M, Lu D, Abe R, Domen K. Efficient Nonsacrificial Water Splitting through Two-Step Photoexcitation by Visible Light using a Modified Oxynitride as a Hydrogen Evolution Photocatalyst. J Am Chem Soc. 2010;132:5858-68.

[3] Lewis NS, Nocera DG. Powering the planet: Chemical challenges in solar energy utilization. Proceedings of the National Academy of Sciences. 2006;103:15729-35.

[4] Tada H, Mitsui T, Kiyonaga T, Akita T, Tanaka K. All-solid-state Z-scheme in CdS–Au–TiO_2 three-component nanojunction system. Nature Mater. 2006;5:782-6.

[5] Tada H, Kiyonaga T, Naya S-i. Rational design and applications of highly efficient reaction systems photocatalyzed by noble metal nanoparticle-loaded titanium(IV) dioxide. Chem Soc Rev. 2009;38:1849.

[6] Zong X, Yan H, Wu G, Ma G, Wen F, Wang L, et al. Enhancement of Photocatalytic H_2 Evolution on CdS by Loading MoS_2 as Cocatalyst under Visible Light Irradiation. J Am Chem Soc. 2008;130:7176-7.

[7] Reece SY, Hamel JA, Sung K, Jarvi TD, Esswein AJ, Pijpers JJH, et al. Wireless Solar Water Splitting Using Silicon-Based Semiconductors and Earth-Abundant Catalysts. Science. 2011;334:645-8.

[8] Zhang X, Ai Z, Jia F, Zhang L. Generalized One-Pot Synthesis, Characterization, and Photocatalytic Activity of Hierarchical BiOX (X = Cl, Br, I) Nanoplate Microspheres. J Phys Chem C. 2008;112:747-53.

[9] Xia J, Yin S, Li H, Xu H, Yan Y, Zhang Q. Self-Assembly and Enhanced Photocatalytic Properties of BiOI Hollow Microspheres via a Reactable Ionic Liquid. Langmuir. 2011;27:1200-6.

[10] Xu H, Yan J, Xu Y, Song Y, Li H, Xia J, et al. Novel visible-light-driven AgX/graphite-like C_3N_4 (X=Br, I) hybrid materials with synergistic photocatalytic activity. Appl Catal, B. 2013;129:182-93.

[11] Osterloh FE. Inorganic Materials as Catalysts for Photochemical Splitting of Water. Chem Mater. 2008;20:35-54.

[12] Kudo A, Miseki Y. Heterogeneous photocatalyst materials for water splitting. Chem Soc Rev. 2009;38:253.

[13] Navarro RM, Alvarez-Galván MC, Villoria de la Mano JA, Al-Zahrani SM, Fierro JLG. A framework for visible-light water splitting. Energy Environm Sci. 2010;3:1865.

[14] Navarro Yerga RM, Álvarez Galván MC, del Valle F, Villoria de la Mano JA, Fierro JLG. Water Splitting on Semiconductor Catalysts under Visible-Light Irradiation. ChemSusChem. 2009;2:471-85.

[15] Wang Y, Wang X, Antonietti M. Polymeric Graphitic Carbon Nitride as a Heterogeneous Organocatalyst: From Photochemistry to Multipurpose Catalysis to Sustainable Chemistry. Angew Chem Int Ed. 2012;51:68-89.

[16] Zhang Y, Ligthart DAJM, Quek X-Y, Gao L, Hensen EJM. Influence of Rh nanoparticle size and composition on the photocatalytic water splitting performance of Rh/graphitic carbon nitride. Int J Hydrogen Energy. 2014;39:11537-46.

[17] Wang X, Maeda K, Thomas A, Takanabe K, Xin G, Carlsson JM, et al. A metal-free polymeric photocatalyst for hydrogen production from water under visible light. Nature Mater. 2008;8:76-80.

[18] Guo Y, Chu S, Yan S, Wang Y, Zou Z. Developing a polymeric semiconductor photocatalyst with visible light response. Chem Commun. 2010;46:7325.

[19] Xing Z, Chen Z, Zong X, Wang L. A new type of carbon nitride-based polymer composite for enhanced photocatalytic hydrogen production. Chem Commun. 2014;50:6762.

[20] Li J, Shen B, Hong Z, Lin B, Gao B, Chen Y. A facile approach to synthesize novel oxygen-doped g-C_3N_4 with superior visible-light photoreactivity. Chem Commun. 2012;48:12017.

[21] Zhang Y, Mori T, Ye J, Antonietti M. Phosphorus-Doped Carbon Nitride Solid: Enhanced Electrical Conductivity and Photocurrent Generation. J Am Chem Soc. 2010;132:6294-5.

[22] Zhang J, Sun J, Maeda K, Domen K, Liu P, Antonietti M, et al. Sulfur-mediated synthesis of carbon nitride: Band-gap engineering and improved functions for photocatalysis. Energy Environm Sci. 2011;4:675.

[23] Wang Y, Di Y, Antonietti M, Li H, Chen X, Wang X. Excellent Visible-Light Photocatalysis of Fluorinated Polymeric Carbon Nitride Solids. Chem Mater. 2010;22:5119-21.

[24] Wang Y, Zhang J, Wang X, Antonietti M, Li H. Boron- and Fluorine-Containing Mesoporous Carbon Nitride Polymers: Metal-Free Catalysts for Cyclohexane Oxidation. Angew Chem Int Ed. 2010;49:3356-9.

[25] Dante RC, Martín-Ramos P, Sánchez-Arévalo FM, Huerta L, Bizarro M, Navas-Gracia LM, et al. Synthesis of crumpled nanosheets of polymeric carbon nitride from melamine cyanurate. J Solid State Chem. 2013;201:153-63.

[26] Tauc J, Grigorovici R, Vancu A. Optical Properties and Electronic Structure of Amorphous Germanium. physica status solidi (b). 1966;15:627-37.

[27] Morales Escobedo A, Mora Sánchez E, Pal U. Use of diffuse reflectance spectroscopy for optical characterization of un-supported nanostructures. Revista Mexicana de Fisica S. 2007;53:18-22.

[28] Niu P, Zhang L, Liu G, Cheng H-M. Graphene-Like Carbon Nitride Nanosheets for Improved Photocatalytic Activities. Adv Funct Mater. 2012;22:4763-70.

[29] Zhang G, Zhang J, Zhang M, Wang X. Polycondensation of thiourea into carbon nitride semiconductors as visible light photocatalysts. J Mater Chem. 2012;22:8083.

[30] Dante RC, Martín-Ramos P, Correa-Guimaraes A, Martín-Gil J. Synthesis of graphitic carbon nitride by reaction of melamine and uric acid. Mater Chem Phys. 2011;130:1094-102.

[31] Foy D, Demazeau G, Florian P, Massiot D, Labrugère C, Goglio G. Modulation of the crystallinity of hydrogenated nitrogen-rich graphitic carbon nitrides. J Solid State Chem. 2009;182:165-71.

[32] Thomas A, Fischer A, Goettmann F, Antonietti M, Müller J-O, Schlögl R, et al. Graphitic carbon nitride materials: variation of structure and morphology and their use as metal-free catalysts. J Mater Chem. 2008;18:4893.

[33] Zhang Y, Liu J, Wu G, Chen W. Porous graphitic carbon nitride synthesized via direct polymerization of urea for efficient sunlight-driven photocatalytic hydrogen production. Nanoscale. 2012;4:5300.

[34] Nemykin VN, Galloni P, Floris B, Barrett CD, Hadt RG, Subbotin RI, et al. Metal-free and transition-metal tetraferrocenylporphyrins part 1: synthesis, characterization, electronic structure, and conformational flexibility of neutral compounds. Dalton Trans. 2008:4233-46.

[35] Ge L, Han C. Synthesis of MWNTs/g-C_3N_4 composite photocatalysts with efficient visible light photocatalytic hydrogen evolution activity. Appl Catal, B. 2012;117–118:268-74.

[36] Xiang Q, Yu J, Jaroniec M. Preparation and Enhanced Visible-Light Photocatalytic H_2-Production Activity of Graphene/C_3N_4 Composites. J Phys Chem C. 2011;115:7355-63.

[37] Sun Y, Li C, Xu Y, Bai H, Yao Z, Shi G. Chemically converted graphene as substrate for immobilizing and enhancing the activity of a polymeric catalyst. Chem Commun. 2010;46:4740.

[38] Ding Z, Chen X, Antonietti M, Wang X. Synthesis of Transition Metal-Modified Carbon Nitride Polymers for Selective Hydrocarbon Oxidation. ChemSusChem. 2011;4:274-81.

[39] Kobayashi K, Tukada H, Kikuchi K, Ikemoto I. NMR and XPS studies of some diselenocarbamates. Bond switch in bis(dimethylselenocarbamoyl) triselenide. Bull Chem Soc Jpn. 1986;59:1741-6.

[40] Jorge AB, Martin DJ, Dhanoa MTS, Rahman AS, Makwana N, Tang J, et al. H_2 and O_2 Evolution from Water Half-Splitting Reactions by Graphitic Carbon Nitride Materials. J Phys Chem C. 2013;117:7178-85.

[41] Yang J, Wang D, Han H, Li C. Roles of Cocatalysts in Photocatalysis and Photoelectrocatalysis. Acc Chem Res. 2013;46:1900-9.

[42] Shi Y, Wan Y, Zhao D. Ordered mesoporous non-oxide materials. Chem Soc Rev. 2011;40:3854.

[43] Liu G, Niu P, Sun C, Smith SC, Chen Z, Lu GQ, et al. Unique Electronic Structure Induced High Photoreactivity of Sulfur-Doped Graphitic C_3N_4. J Am Chem Soc. 2010;132:11642-8.

[44] Ge L, Han C, Xiao X, Guo L, Li Y. Enhanced visible light photocatalytic hydrogen evolution of sulfur-doped polymeric g-C_3N_4 photocatalysts. Mater Res Bull. 2013;48:3919-25.

[45] Zhang L, Liu D, Guan J, Chen X, Guo X, Zhao F, et al. Metal-free g-C_3N_4 photocatalyst by sulfuric acid activation for selective aerobic oxidation of benzyl alcohol under visible light. Mater Res Bull. 2014;59:84-92.

[46] Ma X, Lv Y, Xu J, Liu Y, Zhang R, Zhu Y. A Strategy of Enhancing the Photoactivity of g-C_3N_4 via Doping of Nonmetal Elements: A First-Principles Study. J Phys Chem C. 2012;116:23485-93.

[47] Stolbov S, Zuluaga S. Sulfur doping effects on the electronic and geometric structures of graphitic carbon nitride photocatalyst: insights from first principles. J Phys: Condens Matter. 2013;25:085507.